Development of a new initial-beam-loading compensation system and its application to a free-electron-laser linac

M. Satoh,* T. Koseki, T. Shidara, S. Fukuda, H. Kobayashi, and Y. Kamiya
Accelerator Laboratory, High Energy Accelerator Research Organization (KEK), Ibaraki 305-0801, Japan

N. Nakamura
Synchrotron Radiation Laboratory (SRL), The Institute for Solid State Physics (ISSP), The University of Tokyo, Chiba 277-8581, Japan

T. Sakai, Y. Hayakawa, T. Tanaka, K. Hayakawa, and I. Sato
Laboratory for Electron Beam Research and Application, Institute of Quantum Science, Nihon University, Chiba 274-8501, Japan

S. Miura
Mitsubishi Heavy Industries, Ltd., Hiroshima 729-0393, Japan
(Received 1 August 2008; published 30 January 2009)

We have developed an initial-beam-loading compensation system by a new compensation method, where the system modulates the phase and amplitude of a low-level rf signal simultaneously, thereby optimizing a high-power rf waveform fed to an accelerating structure to compensate the beam energy spread. This compensation system is very compact and can easily be installed in and removed from a klystron system. This system was used in a beam test performed in the 125 MeV electron linac of the Laboratory for Electron Beam Research and Application in Nihon University. Experimental results demonstrate that this system effectively corrects the beam energy spread due to the initial-beam-loading effect. The new compensation method is expected to be effective in the compensation of energy spread in high-intensity and long-pulse beams in electron linacs.

DOI: 10.1103/PhysRevSTAB.12.013501 PACS numbers: 29.20.Ej

I. INTRODUCTION

In high-intensity electron linacs, a long bunch train is accelerated on a long rf pulse. In such a case, the negative longitudinal wake potential increases along the bunch train during one filling time of an accelerating structure, and it causes energy spread within a beam pulse. Its effect is termed the initial-beam-loading (transient beam loading) effect. Because heavy loading results in a large energy spread that may cause a large beam loss, the energy spread should be compensated for by some correction method. The initial-beam-loading effect can be compensated for to a certain extent by using an energy compression system or adjusting the timing of the injection of the beam into the accelerating structure. However, these methods are not sufficiently effective for a large energy spread of the order of several tens of percent.

For the compensation of a large energy spread, the modulation of an rf input to an accelerating structure has been proposed. In this scheme, an accelerating structure is filled with a ramping shaped rf input before beam injection so that the energy gain of each bunch during the transient period is equal to that of each bunch during the steady state. Analytical and numerical calculations of an rf waveform have been performed in many studies [1–6]. In addition, some beam experiments have also been performed [7–10]. In these studies, a high-power rf input is modulated by a two-klystron combination system or a pulse compression system.

It is convenient to compensate the energy spread without using a pulse compressor and a two-klystron combination system. Therefore, we have developed a new initial-beam-loading compensation system that modulates a low-level rf signal [11]. In our compensation method, the phase and amplitude of the low-level rf signal are modulated simultaneously to obtain a desirable modulated rf waveform at a high-power level. The phase modulation and amplitude modulation of the low-level rf signal are carried out on the basis of the total response curve of an amplification system including a preamplifier and high-power klystron. Our system can be installed in and removed from the existing klystron system with great ease because of its simple setup and compact dimensions.

In this paper, we report the new initial-beam-loading compensation system and the results of a beam test. Section II provides a detailed description of the proposed system. Furthermore, we present a brief introduction of the electron linac at the Laboratory for Electron Beam Research and Application (LEBRA) where the beam test was performed. A method for the measurement of the beam energy spread by using our compensation system and the results of the beam test are presented in Sec. III. Finally, we conclude this study in Sec. IV.

*Corresponding author.
masanori.satoh@kek.jp

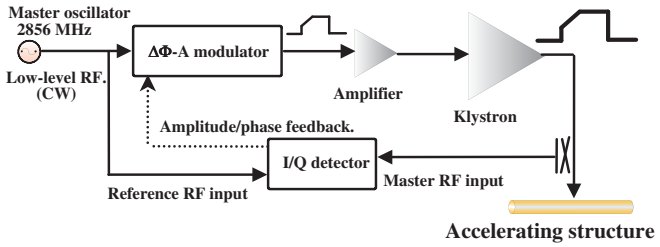

FIG. 1. (Color) Overview of the initial-beam-loading compensation system.

II. SYSTEM DESCRIPTION

A. Overview

Here, we provide a detailed description of the proposed system. Our initial-beam-loading compensation system mainly consists of a $\Delta\Phi$-*A* (phase-to-amplitude) modulator and an inphase/quadrature (I/Q) detector. A simple overview of the system setup is shown in Fig. 1. The key component of this system is the $\Delta\Phi$-*A* modulator. A low-level continuous wave (CW) rf signal is fed to the $\Delta\Phi$-*A* modulator for controlling the amplitude and phase of the rf signal. Then, the modulated rf signal is converted into a pulsed signal and amplified by a preamplifier and a high-power klystron. Finally, the modulated high-power rf signal is fed to the accelerating structure. The output rf signal of the high-power klystron is attenuated and input to the I/Q and rf detectors. These detectors measure the rf phase and amplitude of the klystron output and provide data for the fine-tuning of the modulated rf waveform. The input signal for the $\Delta\Phi$-*A* modulator is fed to the I/Q detector as the reference signal. Further detailed information on the components of the proposed system is provided in the following subsections.

B. $\Delta\Phi$-*A* modulator

In this section, the $\Delta\Phi$-*A* modulator is described briefly. Its detailed description is provided in Ref. [11]. Figure 2 shows the block diagram of the $\Delta\Phi$-*A* modulator. The $\Delta\Phi$-*A* modulator developed by us consists of two high-speed variable phase shifters and two 3 dB power dividers. The hybrid-coupled-type varactor diodes are used as the high-speed phase shifters. After the rf input signal is equally divided into two signals, the two phase shifters shift their phases independently by $\theta 1$ and $\theta 2$, as shown in Fig. 2. Then, the two rf signals are combined into the output signal whose amplitude and phase can be represented by the new vector $(V3, \theta 3)$, and it can be derived from the vector sum of $(V1, \theta 1)$ and $(V2, \theta 2)$. Thus, by simultaneously controlling the two control voltages applied to the phase shifters, we can obtain an output signal with an arbitrary amplitude, phase, and pulse length.

In our system, two 100 MHz programmable arbitrary waveform generators (Pragmatic Instruments, Inc., 2416A) with control voltages in the range of 0 to 10 V are used for

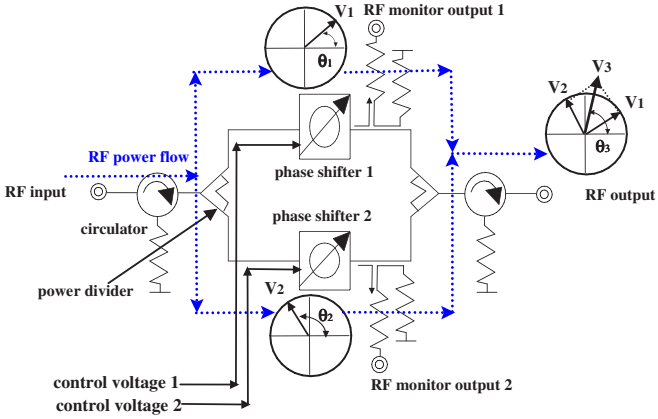

FIG. 2. (Color) Block diagram of the $\Delta\Phi$-*A* modulator.

controlling the two phase shifters, and each generator has a resolution of 12 bits and a rise time of less than 5 ns. The maximum attenuation is greater than 20 dB, and the modulator can convert the input CW signal into a pulse. The changeable range of each phase shifter shown in Fig. 2 is adjusted to approximately ± 110 degrees. We have prepared a lookup table of the phase and amplitude corresponding to the control voltage. The controllable range of the phase and amplitude is shown in Fig. 3.

C. I/Q detector

A high-speed phase detector is highly desirable for achieving accurate initial-beam-loading compensation. For this purpose, I/Q detectors are used for phase detection. The I/Q detector developed by us for use as a high-speed phase detector consists of two double balanced mixers (DBMs), two low-pass filters, a power divider, and a

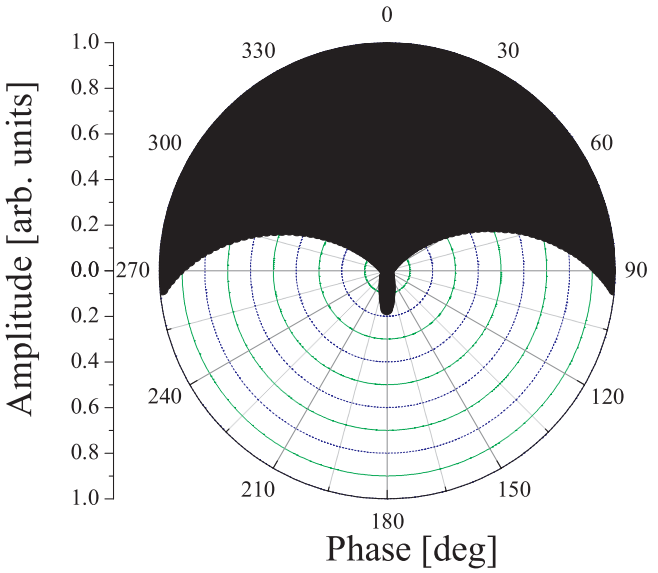

FIG. 3. (Color) Controllable range of the phase and amplitude of the $\Delta\Phi$-A modulator.

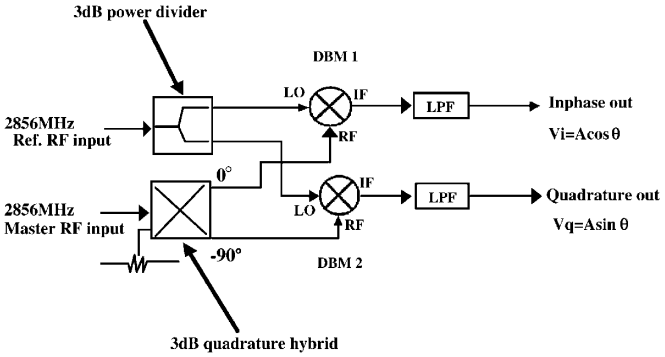

FIG. 4. Block diagram of the fast phase detector (I/Q detector).

3 dB quadrature hybrid, and it divides the rf signal into two output signals with a phase difference of 90 degrees (i.e., in phase and quadrature components). The block diagram and photograph of the high-speed phase detector are shown in Figs. 4 and 5, respectively.

The reference rf signal is divided equally and fed to the LO ports of DBM1 and DBM2. Further, after the master rf signal is divided by the 3 dB quadrature hybrid into two output signals that have equal power but a 90 degrees phase difference, these two signals are input to the rf ports of DBM1 and DBM2. Consequently, we can obtain two DC signals at the IF ports of the two DBMs. One is proportional to $A\cos\theta(=Vi)$ and the other is proportional to $A\sin\theta(=Vq)$, where A and θ are the amplitude of the master rf signal and the phase difference between the master and reference rf signals, respectively. Therefore, we can simultaneously obtain the amplitude A and phase θ of the master rf signal by the following equations:

$$A = \sqrt{V_q^2 + V_i^2} \tag{1}$$

$$\theta = \tan^{-1}\left(\frac{V_q}{V_i}\right). \tag{2}$$

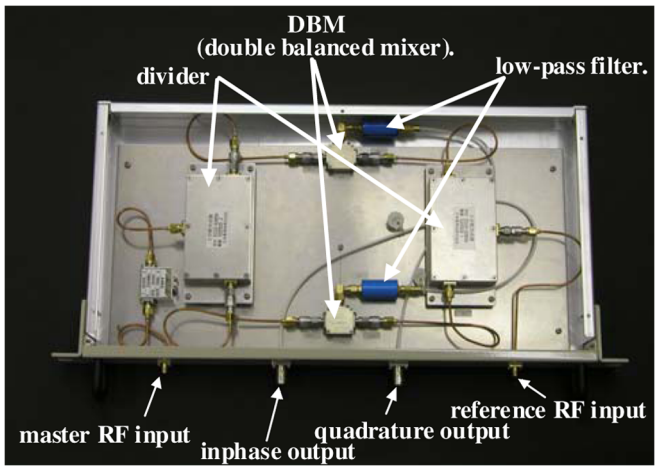

FIG. 5. (Color) Photograph of the fast phase detector (I/Q detector). Its dimensions are 480 mm × 230 mm × 50 mm (W × D × H).

Tests for evaluating the performance of the developed phase detector are performed, and the results show that the response time is less than 10 ns. This performance is adequate since, in this experiment, the $\Delta\Phi$-A modulator is controlled by a 100 MHz frequency.

In order to increase the accuracy of the phase detector, it should be adjusted such that the DC offset voltage is minimum. DC offset voltages are caused by a combination of diode imbalance and transformer asymmetry. Here, the DC offset voltage can be expressed by

$$V_{\mathrm{DC}} = \frac{2\sqrt{50}}{\pi} 10^{[(\mathrm{LO\text{-}IS\text{-}30})/20]-3}, \tag{3}$$

where LO is the level of power applied to the LO port, expressed in dBm, and IS is the LO-to-IF isolation expressed in dB [12]. Using the above expression, when the LO input level is adjusted suitably, we can minimize the DC offset voltage. For this purpose, a variable rf amplifier (HP8347A) is used for varying the rf level input to the reference port. Its output level is from 2 to 20 dBm, and we usually use the output level of around 12 dBm.

After minimizing the DC offset voltage, the fundamental data of the detector, i.e., the phase and amplitude dependences on input rf phase, are measured by using a network analyzer. Here, a simple program in the PC calculates the amplitude and phase value by using Eqs. (1) and (2), respectively. The measurement results are shown in Figs. 6 and 7. They mean phase and amplitude errors of the I/Q detector and could also be used as the calibration data for the phase and amplitude measurements. In our practical use, the range of the input rf phase is less than approximately 30 degrees. From the results shown in Fig. 6, the phase error is considered to be less than ±1 degree. Figure 7 shows that the amplitude error is less than 1% if the input phase is between 90 degrees and 150 degrees. Therefore, the phase detector performs

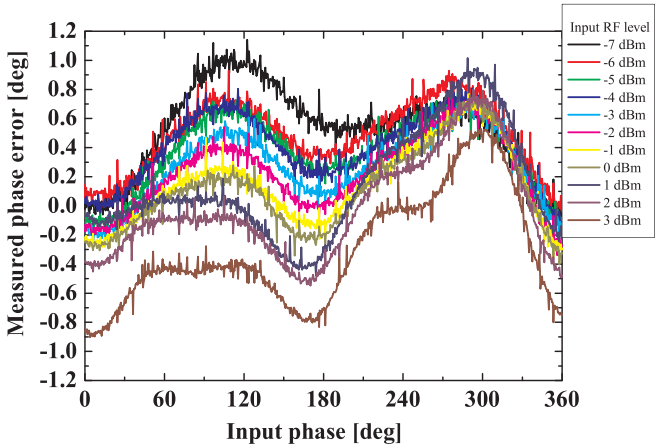

FIG. 6. (Color) Measured phase error with the DBM-based I/Q detector.

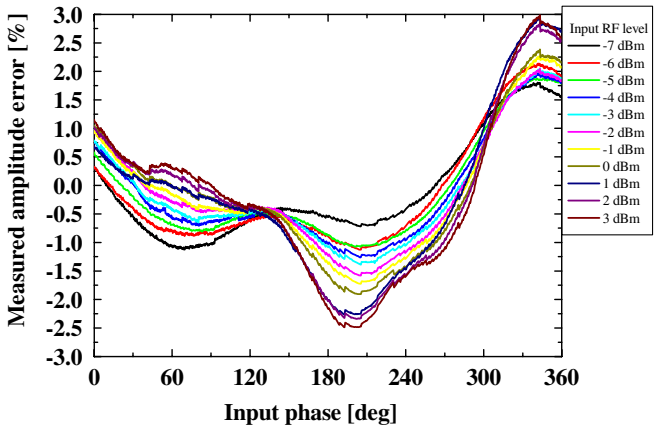

FIG. 7. (Color) Measured amplitude error with the DBM-based I/Q detector.

efficiently as an rf amplitude detector, though an ordinary rf detector was used in our experiments.

D. FEL linac at LEBRA

The compensation system was applied for the beam test to the 125 MeV electron linac at the LEBRA in Nihon University. The layout and photograph of this electron linac are shown in Figs. 8 and 9, respectively.

The LEBRA facility has both a free electron laser (FEL) and a parametric x-ray (PXR) generation system based on the S-band (2856 MHz) 125 MeV electron linac. The electron linac consists of two klystrons, a DC gun, a prebuncher, a buncher, and three 4-m-long accelerating structures, each of which consists of 110 cells. Each klystron unit has an IΦA system and a 900 W solid-state amplifier (class-C). Klystron 1 drives the prebuncher, buncher, and accelerating structure 1 (Acc1). Klystron 2 drives accelerating structures 2 (Acc2) and 3 (Acc3). A multibunch beam with a pulse length of 20 μs is accelerated by a frequency of 2856 MHz. Two bending magnets at the ends of the straight section of the electron linac can switch the beam trajectory into the FEL or the PXR generation system.

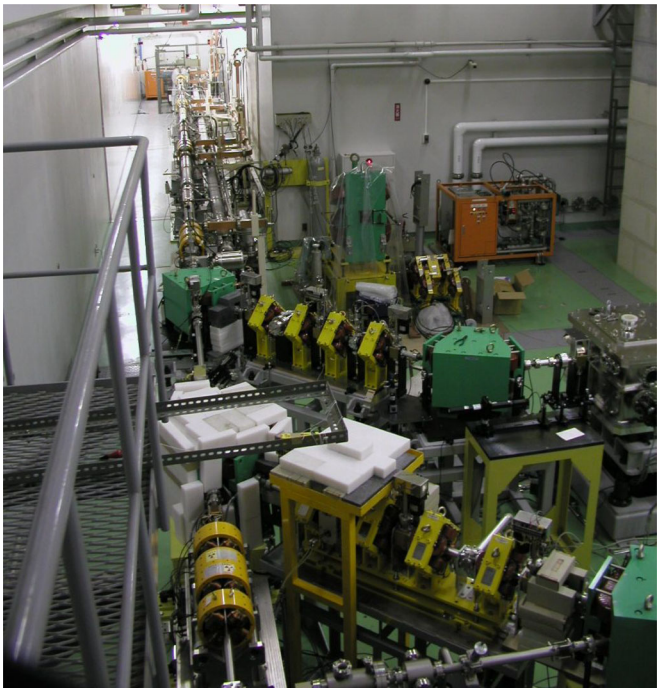

FIG. 9. (Color) Photograph of LEBRA.

The FEL system, whose coverage ranges from the infrared region to the ultraviolet region, was designed and constructed at the LEBRA facility in 1994 [13]. The facility houses a conventional S-band electron linac and a planar undulator with an alternative field of 50 periods. The first lasing of this system was carried out in June 2001 at a wavelength of 1.5 μm by using dielectric mirrors. The PXR generation system was studied simultaneously, and the first light was observed in April 2004. Both the FEL and PXR generation system are utilized in many projects at the LEBRA facility.

III. EXPERIMENT

A. Setup

For the compensation of the energy spread of two accelerating structures (Acc2 and Acc3 in Fig. 1), instead of

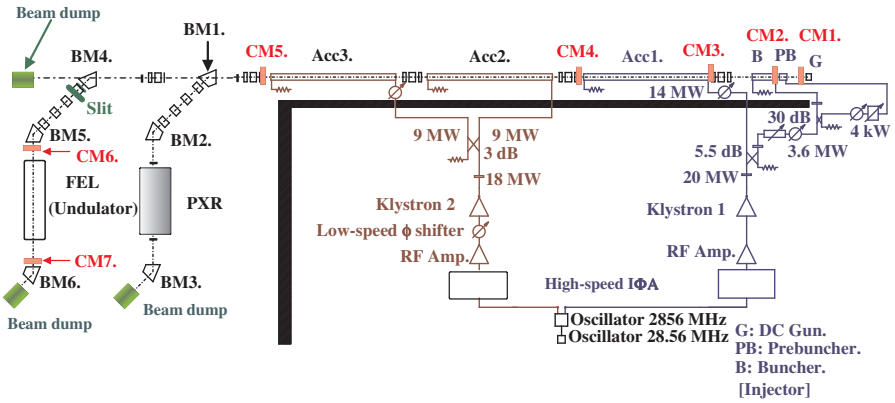

FIG. 8. (Color) Layout of the 125 MeV electron linac at LEBRA.

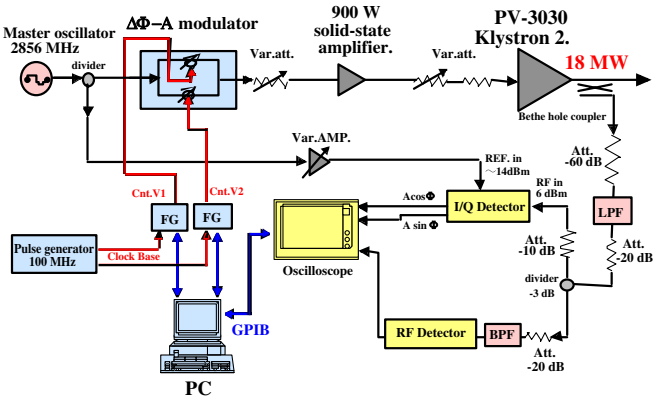

FIG. 10. (Color) Block diagram of the initial-beam-loading compensation system setup in the beam test.

using a high-speed IΦA unit, we installed the ΔΦ-*A* modulation system upstream of solid-state amplifier 2 that drove klystron 2. If the modulator is installed in klystron 1, the ramping profile rf is input to not only the accelerating structure (Acc1) but also the prebuncher and buncher, and it may degrade the bunching operation of the electron beams. Therefore, in this experiment, we aim to compensate for the energy spread caused by only Acc2 and Acc3. Figure 10 shows the block diagram of the initial-beam-loading compensation system used in this beam test.

The beam energy was measured at the FEL beam line of the electron linac at the LEBRA. The method for measuring the beam energy is based on the principle that charged particles with different energies travel on different trajectories in a magnetic field. The relationship between the total energy of the beam and the magnetic field strength can be expressed as

$$E = \sqrt{(eB\rho c)^2 + (m_0c^2)^2} \approx eB\rho c \qquad (E \gg m_0c^2). \tag{4}$$

Using this equation, the energy of the electron beam can be obtained by changing the field strength of the bending magnet.

In the beam test, the beam energy profile along the bunch train was measured by varying the excitation current of the bending magnet BM4. A slit was installed downstream of BM4. If the width of the slit aperture is reduced, we can obtain a higher energy resolution. The transfer matrices of a drift space M_D and a sector-type bending magnet M_B can be expressed as follows:

$$M_D = \begin{pmatrix} 1 & L & 0 \\ 0 & 1 & 0 \\ 0 & 0 & 1 \end{pmatrix} \tag{5}$$

and

$$M_B = \begin{pmatrix} \cos\alpha & \rho\sin\alpha & \rho(1-\cos\alpha) \\ -\frac{1}{\rho}\sin\alpha & \cos\alpha & \sin\alpha \\ 0 & 0 & 1 \end{pmatrix}, \tag{6}$$

where L is the length of the drift space and α and ρ are the bending angle and radius, respectively. Here the vector elements operated on are x_0, x_0', and $\delta_0(=\frac{\Delta p}{p})$, the initial horizontal position, initial angle, and initial momentum deviation, respectively. When an electron with $x_0 = x_0' = 0$ traverses the bending magnet, the momentum deviation, position, and angle at position 1 are given by the following equation:

$$\begin{pmatrix} x_1 \\ x_1' \\ \delta_1 \end{pmatrix} = M_D M_B \begin{pmatrix} x_0 \\ x_0' \\ \delta_0 \end{pmatrix} = \begin{pmatrix} \delta_0\{\rho(1-\cos\alpha) + L\sin\alpha\} \\ \delta_0 \sin\alpha \\ \delta_0 \end{pmatrix}. \tag{7}$$

In the case of our experiment, we use the parameter values of $L = 705$ mm, $\alpha = 45$ degrees, and $\rho = 55$ mm. As a result, Eq. (7) can be rewritten as

$$\begin{pmatrix} x_1 \\ x_1' \\ \delta_1 \end{pmatrix} = \begin{pmatrix} 659.6\delta_0 \\ 0.707\delta_0 \\ \delta_0 \end{pmatrix}. \tag{8}$$

Using the above expression, the width of the slit downstream of BM4 is set to 1 mm, which corresponds to an energy resolution of 0.15%.

B. rf waveform

Assuming that the 100 mA beam is accelerated by a rectangular rf waveform with input powers of 14 MW (Acc1) and 9 MW (Acc2 and Acc3), the dotted black

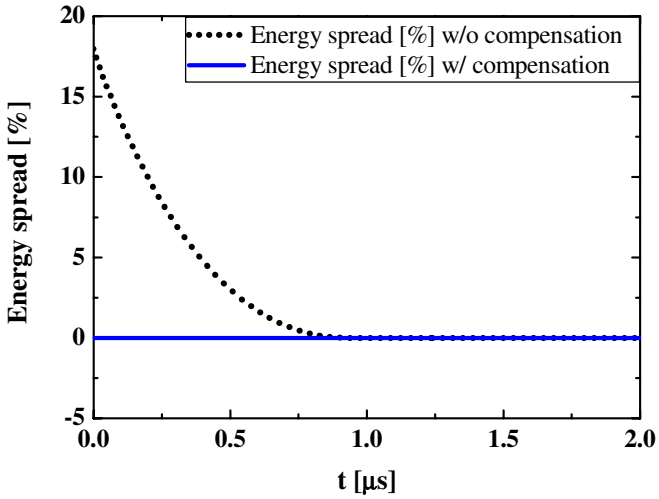

FIG. 11. (Color) Calculated energy spreads without and with compensation.

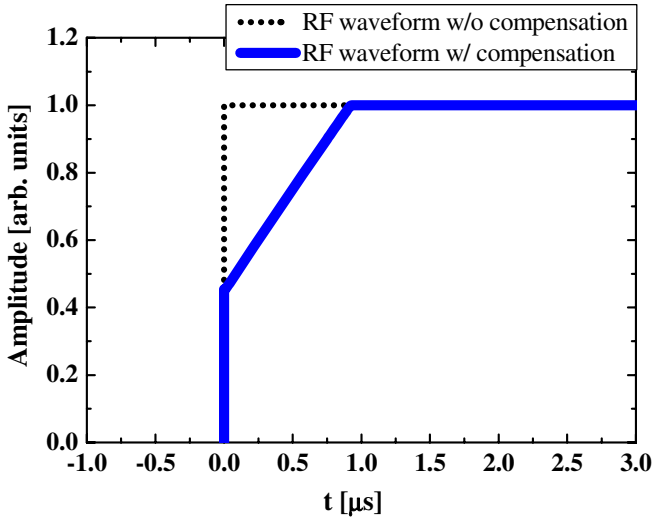

FIG. 12. (Color) Modulated rf waveform for energy spread compensation (solid blue line) and ordinary rectangular waveform profile (dotted black line).

line in Fig. 11 shows the calculated beam energy spread without any initial-beam-loading compensation. By our compensation method, the energy spread can ideally be reduced to 0% from approximately 20%, as shown by the solid blue line in the same figure. In this compensation, the modulated rf waveform shown in Fig. 12 is used. The target ramping rf profile was calculated by using the power flow matrix model employed in Sec. 2.2 of Ref. [11]. The target phase along the rf pulse was set to be constant.

First, we measure the total response curve of the amplification system, which consists of the 900 W solid-state amplifier and the klystron. Using this result, the inverse characteristics of the amplification system and its fitting curve with a sixth-degree polynomial are obtained.

Table I shows the main parameters in this experiment. The output power of klystron 2 is approximately 18 MW, which is divided equally and input to Acc2 and Acc3. By using these parameters and without using any compensation method, the beam energy spread is expected to be approximately 24% downstream of Acc3. The target rf waveform (amplitude profile) shown by the black solid line in Fig. 13 is required to compensate for the energy spread caused by the 100 mA beam current and the 9 MW input power to accelerating structures Acc2 and Acc3. In the target profile between -1 μs and 0 μs, a small rectangular rf waveform is added to the ramping waveform profile after 0 μs since the elimination of an abrupt change in the output power is effective in controlling the amplitude precisely. The final results of the control of the amplitude and phase of the klystron are shown in Figs. 14 and 15, respectively.

From Fig. 14, it can be observed that the amplitude deviation occurs in the first microsecond, though it is much reduced in the next few microseconds. Achieving highly precise amplitude control in the present setup is relatively difficult since the solid-state amplifier shown in Fig. 10 has the performance of a class-C amplifier. In the plot shown in Fig. 15, there is a phase drift of 8 degrees after 1 μs, and this phase drift can be attributed to the phase shift of the solid-state amplifier, caused by its own heat [14]. The final result shows, however, that the phase deviation within the entire pulse is reduced to less than ± 2 degrees.

TABLE I. Main parameters of beam test.

Repetition rate	2 Hz
rf frequency	2856 MHz
Shunt impedance of the accelerating structure	60 MΩ/m
Accelerating structure	4 m × 3 (constant gradient)
Acceleration type	Traveling wave
Attenuation parameter τ	0.627 Np
Filling time t_f	0.935 μs
Q value	13 000
Beam energy gain of steady state	
With compensation	89 MeV
Without compensation	100 MeV
Beam pulse width	2.3 μs
Average beam current	
At the DC gun (CM1)	180 mA
Upstream of Acc1 (CM3)	140 mA
Upstream and downstream of Acc2 and Acc3 (CM4 and CM5)	100 mA
Klystron output power	
Klystron 1 (w/o compensation system)	20 MW
Klystron 2 (w/ compensation system)	18 MW
Input power of accelerating structure	
Acc1	14 MW
Acc2 and Acc3	9 MW

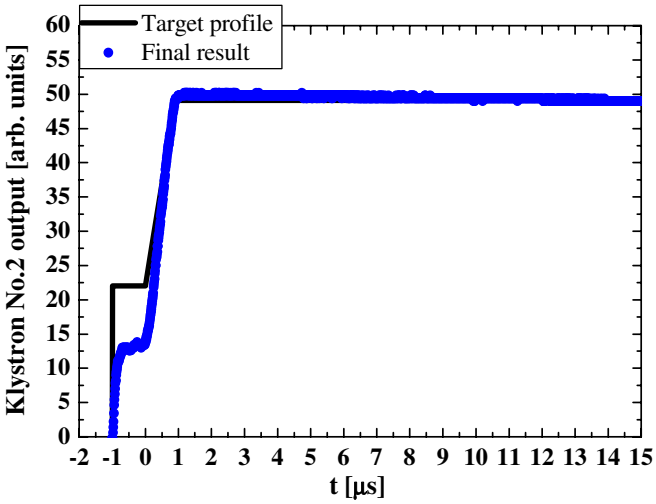

FIG. 13. (Color) Final result of output and target profile (amplitude profile) of klystron 2.

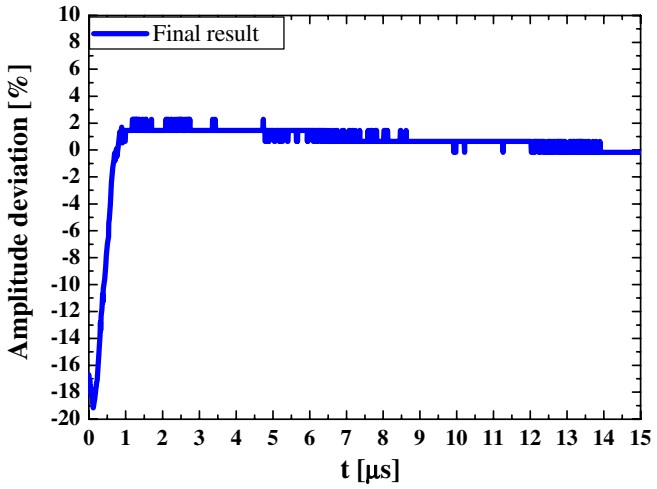

FIG. 14. (Color) Final result of deviation of output of klystron 2 from the target profile (amplitude profile).

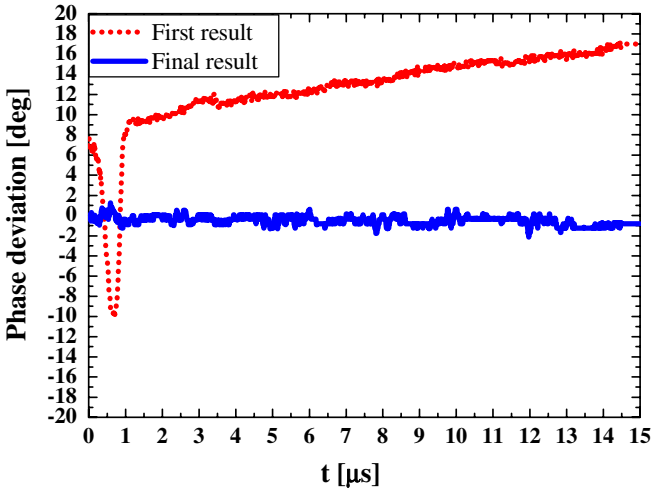

FIG. 15. (Color) First and final results of deviation in the klystron output (phase).

C. Result

The beam energy was measured with and without compensation. In the measurement with compensation, the phase of the klystron output was adjusted to accelerate the beam on the crest of the rf field. After the measurement of the beam energy with compensation, the $\Delta\Phi$-A modulator was removed from amplification system no. 2 and the IΦA unit was installed in place of the modulator for performing the measurement without compensation. During the installation and removal of this modulator, the path and tension of the rf cable changed slightly. Therefore, the absolute beam energies before and after the compensation might be slightly different.

Figure 16 shows the beam current profiles measured at core monitors (CMs) CM3 and CM4. After the beam of 180 mA emitted by the DC gun traverses the prebuncher

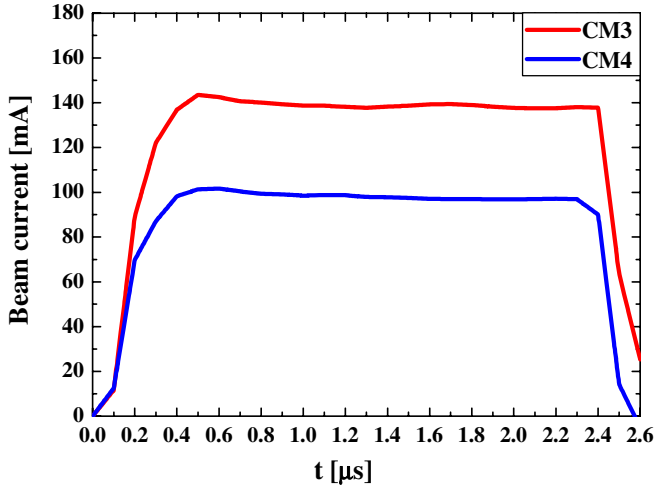

FIG. 16. (Color) Beam current profile measured by core monitors CM3 and CM4.

and buncher for achieving bunching, the beam current reduces to 140 mA upstream of Acc1 because of beam loss. Furthermore, since beam loss also occurs in Acc1 because of imperfect beam bunching conditions, the beam current measured downstream of Acc1 (at CM4) reduces to around 100 mA. After the beam traverses Acc2 and Acc3, the beam of 100 mA still remains at CM5.

The closed black and blue circles in Fig. 17 show the measured beam energy spreads $\Delta E/E$ before and after the initial-beam-loading compensation, respectively, carried out downstream of Acc3. The dotted lines in Fig. 17 show the calculation results obtained from the measured beam current profile shown in Fig. 16 and the klystron output waveform shown in Fig. 13. These numerical calculations were performed using the power flow matrix

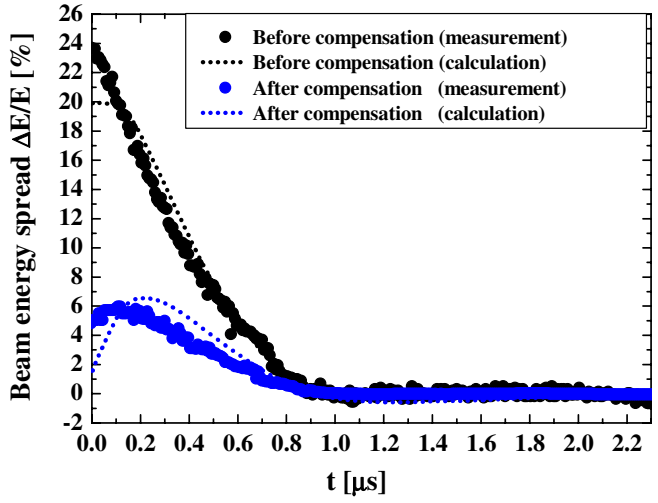

FIG. 17. (Color) Measured and calculated beam energies before (black) and after (blue) the initial-beam-loading compensation downstream of Acc3.

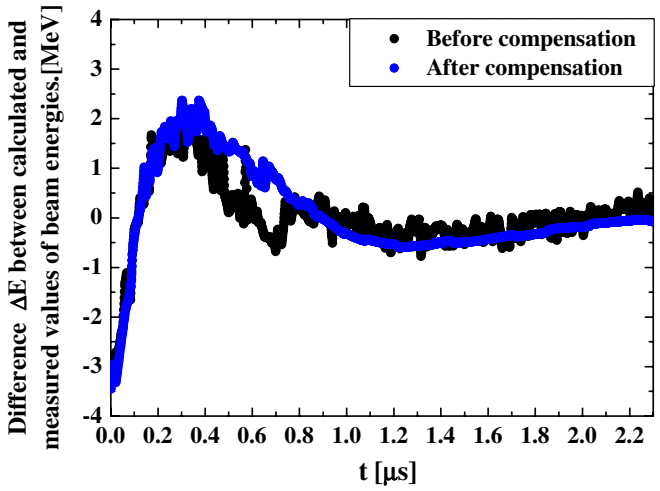

FIG. 18. (Color) Difference between calculated and measured beam energies before and after compensation.

model employed in Ref. [11]. The results of the energy measurement show that the use of our compensation system reduces the energy spread from 24% to 6%. The primary reason for the residual energy spread of 6% after compensation is that the initial-beam-loading effect is not compensated for at Acc1. When the same type of compensation system is installed in klystron 1, the energy spread can be reduced to a significant extent or brought down to almost zero. Alternatively, the energy spread may be further reduced by overcompensating for the beam loading in Acc2 and Acc3 without messing up the prebuncher and buncher rf pulses.

Figure 18 shows the difference between the calculated and measured beam energies before and after compensation. These two profiles are very similar. This similarity suggests that there is a common systematic error in this beam energy calculation and/or measurement. The difference in the beam energies is fairly large at the leading edge of the beam pulse, where the intensity of the beam current drastically increases from zero to the peak value. If there is some measurement error in the beam current profile, particularly at the leading edge of the beam pulse, the calculated beam energies in Fig. 17 can have substantial error, which is considered to be one of the causes of the disagreement between the calculated and measured beam energies.

IV. CONCLUSIONS

A new initial-beam-loading compensation system was developed to compensate for energy spread along a long bunch train in an electron linac. An I/Q detector consisting of two DBMs was introduced to measure the klystron output phase rapidly and accurately. Its response time was less than 10 ns, and it was sufficient for our purpose. It could simultaneously measure the phase and amplitude at high speed, though the amplitude was measured by an ordinary rf detector in this experiment. The phase and amplitude deviations were less than ± 1 degree and $\pm 3\%$, respectively.

A beam test was performed using the developed compensation system at the electron linac of the LEBRA. In this beam test, energy spread compensation was carried out for Acc2 and Acc3. By using the compensation system, the energy spread was reduced from 24% to 6%. The residual energy spread of 6% was caused mainly by Acc1, where the compensation system was not installed. The measured beam energy distribution along the bunch train was in agreement with the distribution calculated from the measured rf power and current profile within a few megaelectron volts. By installing the compensation system in every accelerating structure, the energy spread could be reduced to almost zero. From this result, it is confirmed that our system is effective in compensating for the energy spread in high-intensity and long-pulse electron linacs.

The degree of beam loading can change temporally since the beam current profile varies according to the room temperature drift and/or other factors. Although we did not change the klystron output in this beam test, an rf waveform downstream of the accelerating structure should be monitored and used as a feedback control variable for highly precise compensation. Such a fast feedback method will be developed by using a new control system in the near future.

ACKNOWLEDGMENTS

The authors would like to thank the SRL-ISSP machine group for their support and encouragement in this study.

[1] K. A. Thompson and R. D. Ruth, in *Proceedings of the Particle Accelerator Conference, Washington, DC, 1993* (IEEE, New York, 1993), Vol. 5, pp. 3693–3695.
[2] SLAC Report No. 411, pp. 32–33, 1993.
[3] Z. D. Farkas and P. B. Wilson, SLAC NLC-Note 4, 1994.
[4] C. Nantista and C. Adolphsen, SLAC NLC-Note 25, 1997.
[5] I. V. Syrachev and T. Higo, KEK Report No. 96–8 A, 1996.
[6] T. Shintake, in Proceedings of RF96, Shonan Village Center, Hayama, Kanagawa, Japan, pp. 37–46, 1996.
[7] C. Adolphsen *et al.*, in *Proceedings of the Particle Accelerator Conference, Vancouver, BC, Canada, 1997* (IEEE, New York, 1997), p. 1676.
[8] S. Kashiwagi *et al.*, in Proceedings of the 1998 Linear Accelerator Conference, Chicago, IL, USA, p. 91.
[9] Z. D. Farkas, in Proceedings of the Ninth International Conference on High Energy Accelerators, Stanford, CA, USA, p. 576.
[10] P. B. Wilson, in Proceedings of the 1990 Linear Accelerator Conference, Albuquerque, New Mexico, USA, p. 204.

[11] M. Satoh, T. Matsumoto, T. Shidara, S. Fukuda, H. Kobayashi, Y. Kamiya, N. Nakamura, T. Koseki, and S. Miura, Nucl. Instrum. Methods Phys. Res., Sect. A **538**, 116 (2005).

[12] S. R. Kurtz, Watkins-Johnson Company Tech-notes Vol. 5, No. 1 (1978).

[13] K. Hayakawa, in Proceedings of the 21st Linear Accelerator Meeting in Japan, Tokyo, Japan, 1996, p. 20.

[14] K. Yokoyama, I. Sato, K. Hayakawa, T. Tanaka, K. Sato, Y. Hayakawa, H. Nakazawa, K. Kanno, T. Sakai, and K. Ishiwata, Jpn. J. Appl. Phys. **41**, 4758 (2002).